The 2′-Hydroxyl Group of the Guanosine Nucleophile Donates a Functionally Important Hydrogen Bond in the *Tetrahymena* Ribozyme Reaction†

James L. Hougland,‡,⊥ Raghuvir N. Sengupta,‡ Qing Dai,§ Shirshendu K. Deb,‡,# and Joseph A. Piccirilli*,‡,||,§

Department of Chemistry, Department of Biochemistry and Molecular Biology, and Howard Hughes Medical Institute, The University of Chicago, Chicago, Illinois 60637

Received January 11, 2008; Revised Manuscript Received April 3, 2008

ABSTRACT: In the first step of self-splicing, group I introns utilize an exogenous guanosine nucleophile to attack the 5′-splice site. Removal of the 2′-hydroxyl of this guanosine results in a 10^6-fold loss in activity, indicating that this functional group plays a critical role in catalysis. Biochemical and structural data have shown that this hydroxyl group provides a ligand for one of the catalytic metal ions at the active site. However, whether this hydroxyl group also engages in hydrogen-bonding interactions remains unclear, as attempts to elaborate its function further usually disrupt the interactions with the catalytic metal ion. To address the possibility that this 2′-hydroxyl contributes to catalysis by donating a hydrogen bond, we have used an atomic mutation cycle to probe the functional importance of the guanosine 2′-hydroxyl hydrogen atom. This analysis indicates that, beyond its role as a ligand for a catalytic metal ion, the guanosine 2′-hydroxyl group donates a hydrogen bond in both the ground state and the transition state, thereby contributing to cofactor recognition and catalysis by the intron. Our findings continue an emerging theme in group I intron catalysis: the oxygen atoms at the reaction center form multidentate interactions that function as a cooperative network. The ability to delineate such networks represents a key step in dissecting the complex relationship between RNA structure and catalysis.

The *Tetrahymena* ribozyme, derived from a naturally occurring self-splicing group I intron, has served as a model system for studying biological catalysis of phosphoryl transfer. This ribozyme catalyzes nucleotidyl transfer between an oligonucleotide substrate and guanosine in a reaction that mimics self-splicing (*8, 9*). Extensive biochemical analysis has defined the kinetic pathway for the ribozyme-catalyzed reaction, leading to models for intron/ribozyme structure and catalytic mechanism (reviewed in ref *6*). Crystallographic analysis (*10–13*) of three different group I introns (*Azoarcus*, *Tetrahymena*, and Twort) has provided structures from which to infer the catalytic mechanism and evaluate functional linkages suggested by biochemical data (*14, 15*). The biochemical and structural data generally agree, although some discrepancy remains regarding the number of metal ions present at the active site. Biochemical studies of the *Tetrahymena* ribozyme support a model in which three active site metal ions mediate catalysis (Figure 1A) (*16–21*), whereas crystallographic data obtained from the *Azoarcus* ribozyme suggest a model involving two metal ions at the active site (Figure 1B) (*10, 12*).

The discovery of the self-splicing reaction immediately prompted questions about the manner in which the ribozyme recognizes the guanosine cofactor and activates it for nucleophilic attack. In perhaps the first structure−function analysis of an RNA enzyme, Bass and Cech identified functional groups of the guanosine cofactor required for splicing activity (*22*). Later, mutational analysis of the putative guanosine binding site guided by phylogenetic comparisons led Michel and co-workers to identify nucleotides in the intron's P7 helix that interact with the guanine nucleobase (*23*). Kinetic and thermodynamic analyses of guanosine binding established that the cofactor binds to the ribozyme in two steps (*24*) and, once bound, enhances docking of the oligonucleotide substrate into the ribozyme core (*25*). The recent crystal structures reveal a common architecture for the guanosine binding site composed of three consecutive layers of stacked base−triple interactions, termed the triple base sandwich (*10–13*). In the central layer of the sandwich, the conserved 3′-terminal guanosine of the intron (ωG) forms a base triple with the G264-C311 base-pair as predicted by Michel et al. (*23*). This base triple engenders specificity for the guanosine nucleobase while helping to position its ribose moiety within the active site.

The interactions between the guanosine cofactor and the active site of the ribozyme hold important clues to the catalytic mechanism. The guanosine 2′-hydroxyl was among

† This work was funded by training program support to J.L.H. (GM008720) and R.N.S. (DK070076) from the National Institutes of Health, and a grant to J.A.P. from the Howard Hughes Medical Institute. J.A.P. is an Investigator of the Howard Hughes Medical Institute. J.L.H. was supported in part by the Predoctoral Training Program at the Interface of Chemistry and Biology (5 T32 GM008720-07) at the University of Chicago. R.N.S. was supported by the NIH Undergraduate Training Program in Physical and Chemical Biology (5 T90 DK070076-02) at the University of Chicago.

* To whom correspondence should be addressed. Tel: 773-702-9312. Fax: 773-702-0271. E-mail: jpicciri@uchicago.edu.

‡ Department of Chemistry.

§ Department of Biochemistry and Molecular Biology.

|| Howard Hughes Medical Institute.

⊥ Present address: Department of Chemistry, University of Michigan, Ann Arbor, MI 48109.

Present address: School of Pharmacy and Pharmaceutical Sciences, Purdue University, West Lafayette, IN 47901.

10.1021/bi8000648 CCC: $40.75
Published on Web 06/24/2008

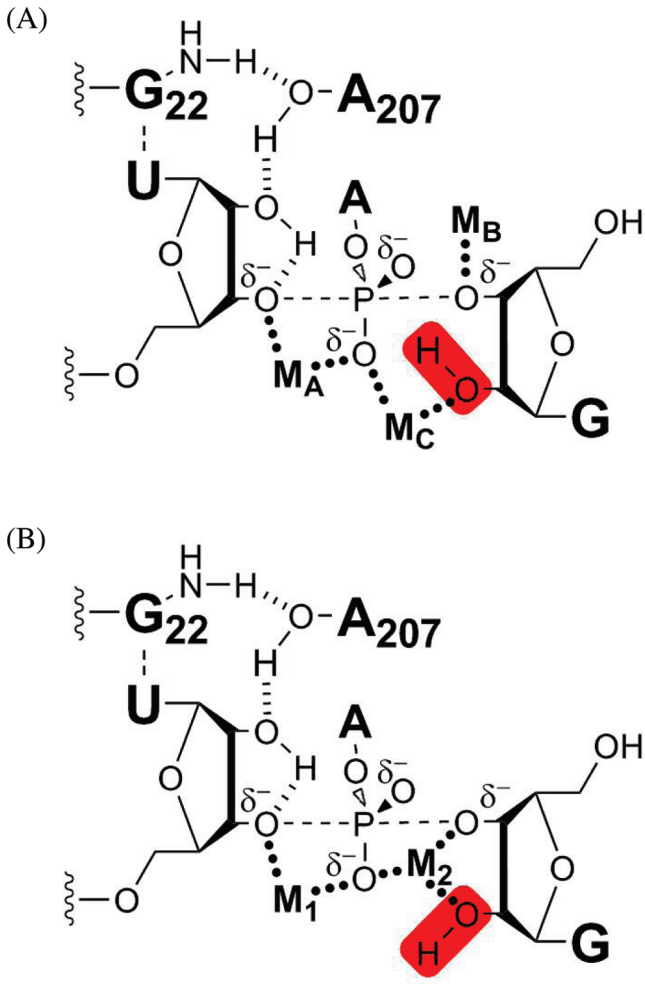

FIGURE 1: Transition-state models for nucleotidyl transfer catalyzed by the *Tetrahymena* group I ribozyme. (A) Model based upon biochemical studies. M_A, M_B, and M_C represent the known catalytic metal ions in the active site. The red rectangle highlights the 2′-hydroxyl group of the guanosine nucleophile under investigation. Hatched lines indicate putative hydrogen bonds, and dots symbolize metal ion coordination. Adapted from ref *21*. (B) Model based upon structural studies. M_1 and M_2 represent the two active-site metal ions observed in the crystal structure of the *Azoarcus* group I intron. Notations are the same as described in A. Adapted from ref *12*.

the first functional groups shown to have importance for catalytic activity; neither 2′-deoxyguanosine nor 2′-methoxyguanosine (G_{OCH_3}[1]) could support intron self-splicing (*26*). Subsequent metal rescue experiments using 2′-aminoguanosine (G_{NH_2}) identified the guanosine 2′-hydroxyl group as a ligand for a metal ion within the active site of the *Tetrahymena* ribozyme (*18, 27*). The crystal structures provide further evidence that an active site metal ion interacts with the 2′-hydroxyl group of the guanosine nucleophile (*10–13*). The absence of this ligand in 2′-deoxyguanosine may explain why 2′-deoxyguanosine cannot support splicing activity. Likewise, the presence of the bulky, hydrophobic methyl group on 2′-methoxyguanosine may disrupt metal ion coordination or have other deleterious steric effects.

[1] Abbreviations: G_{OH}, guanosine; G_{NH_2}, 2′-aminoguanosine; G_{OCH_3}, 2′-methoxyguanosine; G_{NHCH_3}, 2′-methylaminoguanosine; AMC, atomic mutation cycle; NaEPPS, sodium *N*-(2-hydroxyethyl)piperazine-*N*-(3-propanesulfonate); T1, T1 ribonuclease; NHS, sulfosuccinimidyl-6-(biotinamido)hexanoate; TBAF, tetrabutyl ammonium fluoride; E, L-21 *Sca*I *Tetrahymena* group I ribozyme; S, substrate; P, product; MALDI-TOF, time-of-flight matrix-assisted laser desorption ionization.

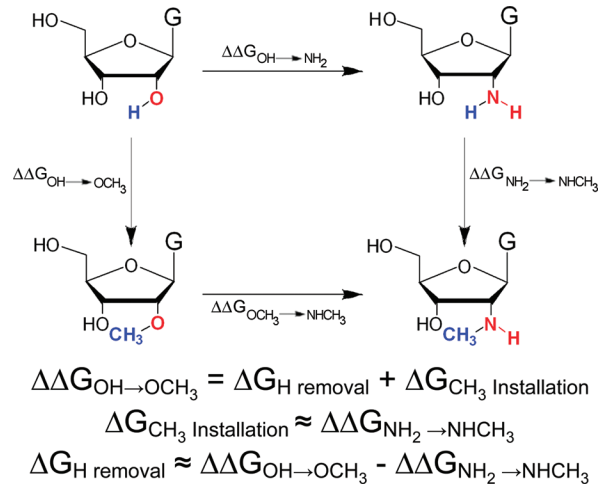

FIGURE 2: Atomic mutation cycle for analysis of the guanosine nucleophile 2′-hydroxyl group.

While these findings strongly support metal ion coordination by the guanosine 2′-hydroxyl group, they do not preclude the possibility that the hydroxyl group also engages in multiple catalytic interactions. 2′-Deoxyguanosine and G_{OCH_3} both lack the ability to donate 2′-hydroxyl-mediated hydrogen bonds. Consequently, the 10^6-fold loss in activity observed for 2′-deoxyguanosine and G_{OCH_3} may also reflect the loss of hydrogen-bonding interactions. However, determining whether the 2′-hydroxyl group participates in hydrogen bonding interactions presents a difficult experimental challenge because common modifications that would alter hydrogen bonding would also likely perturb the interaction with the catalytic metal ion (M_C) (*26, 28*).

To explore whether the guanosine nucleophile 2′-hydroxyl group donates a functionally significant hydrogen bond, we probed the effects of removing hydrogen bond donation ability from this group using an atomic mutation cycle (AMC, Figure 2) (*29–31*). The cycle describes the energetic effects from three atomic mutations (2′-OCH_3, 2′-NH_2, and 2′-$NHCH_3$) relative to the ribonucleotide (2′-OH). Mutation of the 2′-hydroxyl to a 2′-methoxy group (left vertical) replaces the hydrogen atom of the hydroxyl group with a methyl group. A 2′-methoxynucleotide may affect activity through removal of the hydrogen atom ($\Delta G_{H\ removal}$) and/or introduction of the bulky methyl group ($\Delta G_{CH_3\ installation}$), which could cause steric clashes, loss of metal coordination, or other deleterious effects. To resolve the effect of hydrogen atom removal from that of methyl group installation, we used the 2′-amino to 2′-methylamino mutation (right vertical) in which a methyl group replaces one of the hydrogen atoms on an amino group. The 2′-methylaminonucleotide imposes the consequences of the bulky methyl group but, unlike the 2′-methoxynucleotide, also retains a heteroatom-bound hydrogen atom. Therefore, the energetic cost of the 2′-methylamino mutation relative to the 2′-amino mutation provides an independent measure of the effect of methyl group installation ($\Delta G_{CH_3\ installation}$). Energetic differences between the vertical perturbations provide an operational estimate for $\Delta G_{H\ removal}$, and thereby may implicate the 2′-hydroxyl as an important hydrogen bond donor. This analysis has been previously applied with success to the cleavage site uridine in the *Tetrahymena* ribozyme reaction and the cleavage site cytidine of a group II intron reaction (*29, 30*).

Scheme 1: Synthesis of 2′-Methylaminoguanosine (G_{NHCH_3}) and 2′-Dimethylaminoguanosine ($G_{N(CH_3)_2}$) and the Corresponding Phosphoramidites

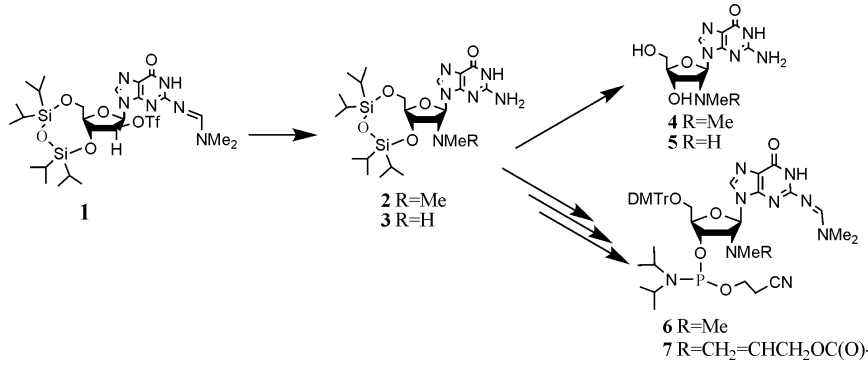

Table 1: Oligonucleotide Substrates Used Herein[a]

abbreviation	position					Oligonucleotide substrate					
	−6	−5	−4	−3	−2	−1	+1	+2	+3	+4	+5
rSA_5	rC	rC	rC	rU	rC	rU	rA	rA	rA	rA	rA
−1d,rSA_5	rC	rC	rC	rU	rC	dU	rA	rA	rA	rA	rA
rP	rC	rC	rC	rU	rC	rU					
−1d,rP	rC	rC	rC	rU	rC	dT					
$CUCG_{OH}A$			rC	rU	rC	G_{OH}	rA				
$CUCG_{OCH_3}A$			rC	rU	rC	G_{OCH_3}	rA				
$CUCG_{NH_2}A$			rC	rU	rC	G_{NH_2}	rA				
$CUCG_{NHCH_3}A$			rC	rU	rC	G_{NHCH_3}	rA				
$CUCG_{N(CH_3)_2}A$			rC	rU	rC	$G_{N(CH_3)_2}$	rA				

[a] r = 2′-OH; d = 2′-H.

We herein present evidence that the guanosine cofactor's 2′-hydroxyl group donates a hydrogen bond in both the ground and transition states of the *Tetrahymena* ribozyme reaction. Our findings further define the features that contribute to group I intron substrate recognition and catalysis and may lead to new constraints for structural models of the *Tetrahymena* ribozyme active site.

MATERIALS AND METHODS

Materials. L-21 *Sca*I ribozyme (E) was transcribed as previously described (*9*). 2′-Methoxyguanosine (G_{OCH_3}) was purchased from ChemGenes and was HPLC purified as detailed below. 2′-Aminoguanosine (G_{NH_2}) was prepared as previously described (*32*). 2′-Methylaminoguanosine (G_{NHCH_3}) and 2′-dimethylaminoguanosine ($G_{N(CH_3)_2}$) were synthesized as described below. Oligonucleotide substrates without G_{NH_2}, G_{NHCH_3}, and $G_{N(CH_3)_2}$ were purchased from Dharmacon (Lafayette, CO) and deprotected according to the manufacturer's protocol.

Synthesis of 2′-Aminoguanosine (G_{NH_2}) Phosphoramidite and $CUCG_{NH_2}A$. The phosphoramidite of G_{NH_2} was synthesized and incorporated into an oligonucleotide as previously reported (*32*).

Synthesis of 2′-Methylaminoguanosine (G_{NHCH_3}) and 2′-Dimethylaminoguanosine ($G_{N(CH_3)_2}$) and Their Incorporation into Oligonucleotides. We synthesized 2′-methylaminoguanosine (G_{NHCH_3}, (**5**)) and 2′-dimethylaminoguanosine ($G_{N(CH_3)_2}$, (**4**)) in which the 2′-nitrogen atom carries one and two methyl groups, respectively (Scheme 1). Briefly, a 2′-triflate derivative (**1**) was treated with dimethylamine or methylamine to give **2** or **3**, respectively. Following TBAF treatment to remove the 2′,5′-silyl protecting group, **2** and **3** were transformed to the corresponding phosphoramidites, **6** and **7**, and incorporated into the oligonucleotide sequence CUCGA. The identities of the modified oligonucleotides were confirmed through MALDI-TOF mass spectrometry. A more detailed synthetic description will be published elsewhere (Dai, Q., Deb, S. K., Sengupta, R. N., and Piccirilli, J.A., unpublished experiments).

HPLC Purification of G_{OCH_3} and G_{NHCH_3}. G_{OCH_3} and G_{NHCH_3} were HPLC purified on a C18 reverse phase semipreparative column (Dionex 201SP510) using a gradient of acetonitrile in 0.1 M triethylammonium acetate buffer (0−20% acetonitrile over 30 min). Buffers at pH 7 and 5.9 were used for G_{OCH_3} and G_{NHCH_3} purification, respectively. Buffer was removed from HPLC purified samples by repeated drying and aqueous resuspension cycles in the Speedvac. Upon dissolution in water, nucleoside concentrations were quantitated by UV absorbance at 260 nm using the extinction coefficient for guanosine ($\epsilon_{260} = 11.7 \times 10^3\ M^{-1}\ cm^{-1}$).

Substrate Preparation. Crude oligonucleotide substrates were either 5′-^{32}P-radiolabeled using [γ-^{32}P]ATP (Perkin-Elmer) and T4 polynucleotide kinase (New England Biolabs) or 3′-labeled using [α-^{32}P]CoTP (Perkin-Elmer) and poly-A polymerase (US Biochemicals) according to manufacturer's protocols and subsequently purified on a 20% nondenaturing polyacrylamide gel. The band corresponding to the full-length substrate was visualized by autoradiography, excised, and eluted at 4 °C overnight into water. Substrates were either used directly with no further purification or ethanol precipitated following elution. Both methods had no effect on the rate of reaction (*7*).

Initial Cleavage Activity Assay and Product Analysis. Guanosine analogues (2 mM) were incubated with 3′-labeled rSA_5 substrate (Table 1) in the presence of saturating E [20−50 nM, K_d^S < 1 nM], 10 mM $MgCl_2$, and 50 mM NaEPPS at pH 8 at 30 °C for 1 h. For T1 cleavage, T1

ribonuclease (10 units) was added to the reaction mixture after 1 h, and the resulting reaction mixture was then incubated at 37 °C for 20 min. For acylation of free 2′-amino groups by sulfosuccinimidyl-6-(biotinamido)hexanoate (NHS), modification was performed under previously reported conditions (*32, 33*). Reaction products were analyzed by 20% denaturing PAGE and visualized by using a Phosphorimager (Molecular Dynamics).

General Reaction Conditions for Forward Cleavage Reactions. All forward cleavage reactions, unless noted otherwise, were performed at 30 °C in 50 mM NaEPPS buffer, pH 8.0, 10 mM $MgCl_2$, and 20−50 nM E. All reactions without $MnCl_2$ present included 0.1 mM EDTA. Reaction mixtures (without radiolabeled substrate) were preincubated at 50 °C for 30 min to renature the ribozyme. The mixtures were then incubated at 30 °C for 5 min, followed by initiation of reaction by addition of substrate. Aliquots (6 × 1 μL) were taken at specified time points and were quenched by the addition of 4 equivalents of stop solution (7 M urea, 50 mM EDTA, 0.3% bromophenol blue, 0.3% xylene cyanol, 0.5 × TBE). Substrate and product were separated by 20% denaturing PAGE. The relative concentrations of substrate and product at each time point were quantitated by using a Phosphorimager (Molecular Dynamics). Good first-order fits to the data were obtained (Kaleidagraph). All reported reaction rates, rate constants, and equilibrium constants are the average of at least three independent determinations; reported errors are one standard deviation from the mean.

General Reaction Conditions for the Reverse Cleavage Reaction. All reverse reactions, unless noted otherwise, were performed at 30 °C in 50 mM NaEPPS buffer, pH 8.0, 50 mM $MgCl_2$, 0.1 mM EDTA, 1 μM E, and 2 μM rP or −1d,rP (Table 1). Reverse reactions were performed and analyzed similarly to the forward cleavage reactions (see above).

Activity Titrations with Guanosine Analogues. Cleavage of the −1d,rSA_5 substrate (Table 1) was monitored under $(E\cdot S)_C$ reaction conditions at pH 8 as described above. As chemistry is rate-limiting with the −1d,rSA_5 substrate (*34*), dissociation constants and $(k_c/K_m)^{G(2'X)}$ values for G_{OH} and G_{NH_2} were obtained from standard Michaelis−Menten fits to plots of observed rates versus guanosine analogue concentration. The measured dissociation constants were in agreement with literature values (*18*). In titrations with G_{NHCH_3}, a linear fit of observed rate versus G_{NHCH_3} concentrations was employed at low G_{NHCH_3} concentrations to obtain a value for $(k_c/K_m)^{G(2'NHCH_3)}$. Over the full range of G_{NHCH_3} concentrations tested, the data were fit to a model describing both G_{NHCH_3} cleavage and substrate inhibition, as described in Supporting Information.

Inhibition Assays with G_{OCH_3} and G_{NHCH_3}. G_{OCH_3} inhibition of −1d,rSA_5 substrate cleavage by G_{OH} was measured under $(k_c/K_m)^{G(2'X)}$ conditions [saturating E (20−50 nM, K_d^S < 1 nM), 12 μM G (K_d^G = 77 ± 3 μM)]. The normalized reaction rate (k^{norm}, defined as the observed cleavage rate in the presence of a given G_{OCH_3} concentration divided by the observed cleavage rate in the absence of G_{OCH_3}) was then used to calculate K_i as shown in eq 1.

$$K_i = \frac{(k^{norm}\cdot[G_{OCH_3}])}{(1-k^{norm})} \quad (1)$$

G_{NHCH_3} inhibition of −1d,rSA_5 substrate cleavage by guanosine was also measured under $(k_c/K_m)^{G(2'X)}$ conditions [saturating E (20−50 nM, K_d^S < 1 nM), 12 μM G (K_d^G = 77 ± 3 μM)]. The observed reaction rate was plotted as a function of G_{NHCH_3} concentration, and the resulting inhibition profile was fit to eq 2, derived from a model describing both competitive inhibition and substrate inhibition as described in Supporting Information.

$$k_{obs} = k_0\left(1-\left(\frac{[G_{NHCH_3}]}{K_{i,1}+[G_{NHCH_3}]}\right)\right)\left(1-\left(\frac{[G_{NHCH_3}]^n}{(K_{i,2})^n+[G_{NHCH_3}]^n}\right)\right) \quad (2)$$

RESULTS

2′-Methylaminoguanosine (G_{NHCH_3}) Acts as a Nucleophile in the Tetrahymena Ribozyme-Catalyzed Cleavage Reaction. For atomic mutation cycle analysis of the guanosine 2′-hydroxyl group to be informative, G_{NHCH_3} must both bind to the ribozyme and serve as a competent nucleophile. In initial assays, we treated the products of the ribozyme reaction with T1 ribonuclease (T1) to distinguish cleavage activity by 2′-methoxyguanosine (G_{OCH_3}) and G_{NHCH_3} from cleavage due to contaminating G_{OH}. T1 exclusively cleaves after guanosine residues bearing 2′-hydroxyl groups. Similarly, to distinguish cleavage activity by G_{NHCH_3} from contaminating G_{NH_2}, we used *N*-hydroxysuccinimidobiotin (NHS), which biotinylates primary amino groups only. In ribozyme reactions, G_{NHCH_3} efficiently cleaved an all-ribose substrate (rSA_5, Table 1) under conditions where G_{OCH_3} exhibited no detectable cleavage activity (i.e., failed to produce a T1 ribonuclease resistant cleavage product) (Figure 3). The 3′-radiolabeled cleavage product formed upon incubation with G_{NHCH_3} resisted modification by both T1 ribonuclease and NHS, consistent with the presence of a 2′-methylaminonucleotide (*32, 33*). As independent confirmation that G_{NHCH_3} can act as a cofactor, we synthesized a substrate analogue, $CUCG_{NHCH_3}A$, bearing G_{NHCH_3} at the cleavage site and showed that it undergoes ribozyme-catalyzed (reverse) reaction with CCCUCU (see below). As the 2′-OCH_3 and 2′-$NHCH_3$ groups have similar steric volume and hydrophobicity (*29*), the slower reactivity of G_{OCH_3} compared to that of G_{NHCH_3} presumably arises from other factors such as disruption of the interaction with M_C or the inability of the 2′-OCH_3 group to donate a hydrogen bond.

Manganese Rescues Reactivity of G_{NHCH_3}. To test whether the presence of the methyl group disrupts M_C coordination to the guanosine 2′-hydroxyl, we measured Mn^{2+} stimulation of G_{NHCH_3} and G_{NH_2} reactivity relative to guanosine (G_{OH}) under $(k_c/K_m)^{G(2'X)}$ conditions using metal rescue assays described previously (*18*). In a background of 10 mM Mg^{2+}, the addition of Mn^{2+} specifically stimulates substrate cleavage by both G_{NH_2} and G_{NHCH_3} (Figure 4), consistent with a transition-state interaction between a Mn^{2+} ion and the 2′-nitrogen atom of G_{NH_2} and G_{NHCH_3}. The Mn^{2+} stimulation of G_{NH_2} and G_{NHCH_3} occurs with the same Mn^{2+} concentration dependence ($K_{d,app}^{Mn,\ E\cdot S}$ = 0.38 and 0.46 mM, respectively; Figure 4), suggesting that the rescuing metal ion binds to the same binding site on the ribozyme (the M_c site). We conclude that, despite the presence of the methyl group, G_{NHCH_3} uses its 2′-nitrogen atom to interact with M_C in the transition state in the same manner as that shown previously for G_{NH_2} (*18*). On the basis of this conclusion, we infer that

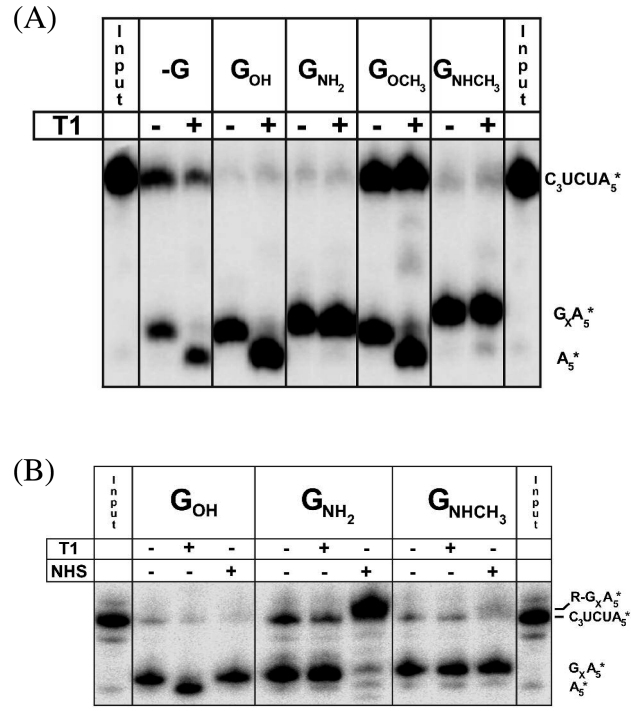

FIGURE 3: Ribozyme-catalyzed nucleotidyl transfer to guanosine analogues. (A) Product analysis by T1 ribonuclease digestion. The digestion of the cleaved product band in the G_{OCH_3} lanes by T1 ($G_{OH}A_5 \rightarrow A_5$) indicates that this cleavage is due to reaction with a small amount of contaminating guanosine, as a product containing G_{OCH_3} would be resistant to T1 digestion. (B) Product analysis by NHS-biotin modification. The resistance of the G_{NHCH_3} induced product to both T1 digestion and NHS-biotin modification shows that the product arises from the reaction of G_{NHCH_3} itself rather from any contaminating G_{OH} or G_{NH_2}. Guanosine analogues (2 mM) were incubated with 3′-labeled rSA_5 substrate in the presence of saturating E [20−50 nM, K_d^S < 1 nM], 10 mM $MgCl_2$, and 50 mM NaEPPS at pH 8 at 30 °C for 1 h.

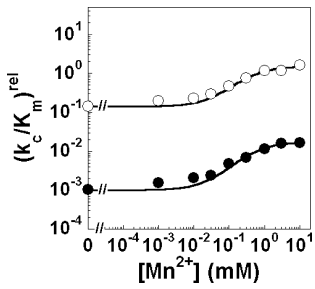

FIGURE 4: Mn^{2+} rescues substrate cleavage by G_{NHCH_3}. Plot of $(k_c/K_m)^{rel}$ $[(k_c/K_m)^{G(2'X)}/(k_c/K_m)^{G(2'OH)}]$ versus Mn^{2+} concentration for G_{NH_2} (○) and G_{NHCH_3} (●). The data are fit to a model for specific stimulation of G_{NH_2} and G_{NHCH_3} reactivity by a single Mn^{2+} ion, as described in the Supporting Information. The rescuing Mn^{2+} ion binds to the ribozyme with $K_{d,app}^{Mn,\,E\cdot S} = 0.46 \pm 0.06$ mM and $K_{d,app}^{Mn,\,E\cdot S} = 0.38 \pm 0.10$ mM as assayed by reaction with G_{NHCH_3} and G_{NH_2}, respectively, consistent with Mn^{2+} occupancy at the M_C binding site (*19*).

the presence of the methyl group on G_{OCH_3} does not interfere with metal ion coordination. Therefore, the greatly diminished reactivity of G_{OCH_3} presumably arises from factors other than the loss of metal coordination.[2,3]

[2] The absence of activity with G_{OCH_3} could also reflect weakened ligand−donor properties of the methyl ether relative to the hydroxyl group. However, experiments have shown that, at least in the gas phase, the methyl ether acts as a stronger ligand donor than does the corresponding alcohol (*1, 2*).

Table 2: Binding Affinities of Guanosine Analogues[a]

analogue	$K_d^{G(2'X)}$ (μM)	$K_d^{G(2'X)}/K_d^{G(2'OH)}$
G_{OH}	77 ± 3	1
G_{OCH_3}	26,000 ± 1,000	340
G_{NH_2}	276 ± 8	3.6
G_{NHCH_3}	2700 ± 300	35

[a] Binding affinities for G_{OH} and G_{NH_2} were measured by titration of ribozyme cleavage activity; binding affinities for G_{OCH_3} and G_{NHCH_3} were measured by inhibition of ribozyme cleavage activity in the presence of subsaturating guanosine, as detailed in Materials and Methods.

Atomic Mutation Cycle Analysis of Guanosine Binding. Effects from methyl group incorporation and hydrogen atom removal at the guanosine 2′-position can manifest in both the ground state and transition state of the ribozyme reaction. To investigate the ground-state effects from the AMC modifications of the guanosine 2′-hydroxyl, we assayed binding of the four guanosine analogues to the $(E\cdot S)_C$ complex.[4] G_{OH} and G_{NH_2} binding were measured by monitoring the cleavage activity of the $(E\cdot S)_C$ complex as a function of G_{OH} or G_{NH_2} concentration, which yielded dissociation constants consistent with literature values (Table 2 and data not shown) (*18*). Because of the absence of cleavage activity with G_{OCH_3}, the dissociation constant for this analogue was measured by a competitive inhibition assay, in which reaction of the $(E\cdot S)_C$ complex in the presence of subsaturating G_{OH} $[(E\cdot S)_C + G_{OH} \rightarrow (E\cdot S\cdot G_{OH})_C^{\ddagger}]$ was measured as a function of increasing G_{OCH_3} concentration (Figure 5A). G_{OCH_3} inhibited the reaction with a K_i value of 26 mM, approximately 340-fold larger than the K_d for G_{OH} (77 μM), indicating that replacement of the 2′-hydroxyl group with a methoxy group destabilizes binding to the ground-state $(E\cdot S)_C$ complex by 3.5 kcal/mol ($\Delta\Delta G_{OH\rightarrow OCH_3}^{binding}$; Figure 6B). Comparison of the binding affinities for oligonucleotides $CUCG_{OH}$ and $CUCG_{OCH_3}$, wherein the lengthening of the guanosine nucleophile to $CUCG_{2'X}$ enhances binding relative to $G_{2'X}$ alone (*28*), yields similar results (see Supporting Information).

To delineate the contributions of methyl group incorporation and hydrogen atom removal to the loss in binding affinity observed upon 2′-methoxy substitution, we compared the binding affinity of G_{NHCH_3} to that of G_{NH_2}. This comparison provides an estimate for the effect of the methyl group on binding of the guanosine analogue in the context of a heteroatom-bound hydrogen atom. We first attempted to measure the binding affinity of G_{NHCH_3} to the $(E\cdot S)_C$ complex through an activity titration of substrate cleavage, but substrate inhibition at high G_{NHCH_3} concentrations precluded an accurate K_d determination (Figure 5B).[5] However, as substrate cleavage by G_{NHCH_3} occurs much slower than does

[3] The addition of Mn^{2+} also stimulates G_{OCH_3} reactivity (see Supporting Information). However, since Mn^{2+} is known to induce nonspecific effects (*3*) and Frederiksen, J. K., Herschlag, D., and Piccirilli, J. A., unpublished experiments), we chose to focus on AMC analysis of the guanosine 2′-hydroxyl group in a Mg^{2+} background.

[4] The substrate, S, binds to E by forming Watson−Crick base pairs with the ribozyme's internal guide sequence to form the P1 helix; this complex is referred to as the "open complex" or $(E\cdot S)_O$ (*4, 5*). Tertiary interactions allow the P1 helix to dock into the ribozyme and form the closed complex or $(E\cdot S)_C$ (see ref *6* and references therein). In these experiments, only substrates that bind primarily in the closed complex were used (*7*).

[5] We have observed similar substrate inhibition at high concentrations of G_{NH_2} (Hougland, J. L., and Piccirilli, J. A., unpublished data). The physical basis for this inhibition is unknown.

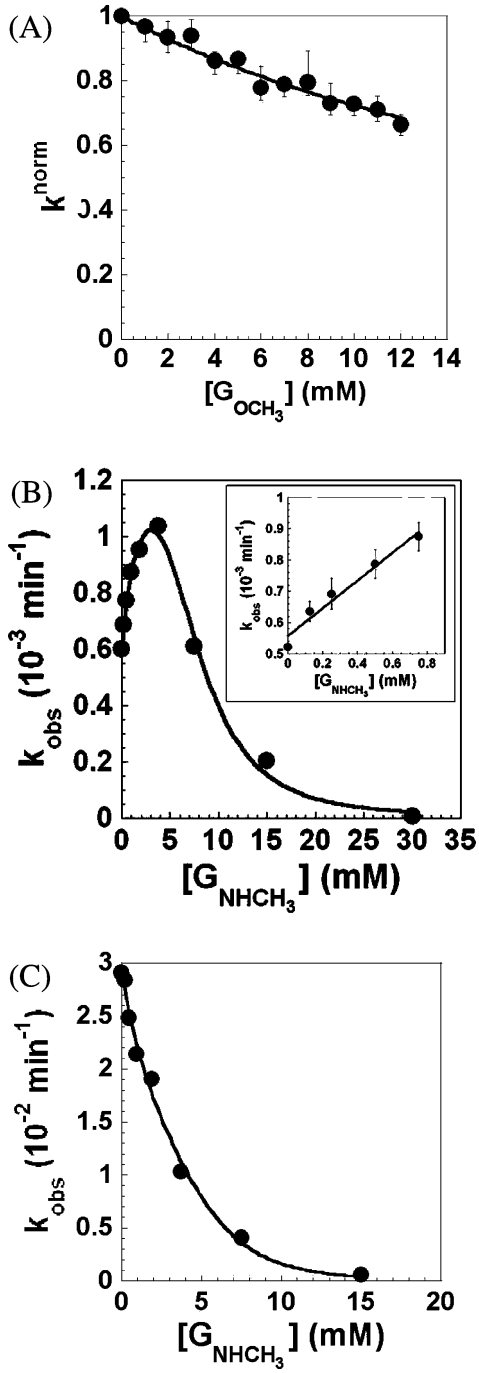

FIGURE 5: G_{OCH_3} and G_{NHCH_3} bind weakly to the enzyme−substrate closed complex. (A) G_{OCH_3} binding affinity to $(E \cdot S)_C$ as measured by inhibition. G_{OCH_3} inhibition of −1d,rSA_5 substrate cleavage was measured and analyzed as described in Materials and Methods to yield a K_i for G_{OCH_3} of 26 ± 1 mM. (B) Activity titration with G_{NHCH_3} reveals substrate inhibition. Activity titration of −1d,rSA_5 substrate cleavage with G_{NHCH_3} exhibits both stimulatory and inhibitory regimes, with severe inhibition observed at high concentrations of G_{NHCH_3}. In the stimulatory regime of the G_{NHCH_3} activity titration, a linear fit yields $(k_c/K_m)^{G(2'NHCH_3)} = 0.44 \pm 0.05$ M^{-1} min^{-1} (inset). (C) G_{NHCH_3} binding affinity to $(E \cdot S)_C$ measured by inhibition of guanosine-mediated substrate cleavage. G_{NHCH_3} inhibition of −1d,rSA_5 substrate cleavage was measured as described in Materials and Methods. The data are fit to a model for both competitive inhibition and cooperative substrate inhibition by G_{NHCH_3} (see Supporting Information). Specific inhibition occurs with a $K_i = 2700 \pm 300$ μM, and substrate inhibition occurs with $K_i = 6830 \pm 50$ μM and $n = 3$.

cleavage by G_{OH}, we monitored G_{NHCH_3} binding by inhibition of the reaction, $(E \cdot S)_C + G_{OH} \rightarrow (E \cdot S \cdot G_{OH})^{\ddagger}_C$. We fit the observed inhibition by G_{NHCH_3} to a model allowing for both competitive inhibition and noncompetitive substrate inhibition (Figure 5C and Supporting Information). The K_i for competitive inhibition by G_{NHCH_3} is 2700 μM, approximately 10-fold larger than the dissociation constant for G_{NH_2} (276 μM, Table 2), suggesting that the methyl group destabilizes binding to the $(E \cdot S)_C$ complex by ∼ 1.4 kcal/mol ($\Delta\Delta G^{binding}_{NH_2 \rightarrow NHCH_3}$, Figure 6B). The difference in the energetic penalties for the 2′-OH to 2′-OCH_3 mutation and the 2′-NH_2 to 2′-$NHCH_3$ mutation yields a $\Delta G^{binding}_{H\ removal}$ of 2.1 kcal/mol, suggesting that G_{OCH_3} destabilizes guanosine binding through the absence of the hydrogen atom (Figure 6B). On the basis of this analysis, we infer that the hydrogen atom of the guanosine 2′-hydroxyl plays a functionally important role in guanosine binding, presumably by donating a hydrogen bond.

Atomic Mutation Cycle Analysis of Guanosine Reactivity. To evaluate the transition-state effects for hydrogen atom removal ($\Delta G^{chemistry}_{H\ removal}$) at the guanosine nucleophile 2′-hydroxyl, we measured the reactivity of the guanosine analogues under subsaturating $[(k_c/K_m)^{G(2'X)}]$ conditions. In the presence of saturating ribozyme and an oligonucleotide substrate that binds to the ribozyme primarily in the closed complex (−1d,rSA_5, Table 1), $(k_c/K_m)^{G(2'X)}$ values monitor the overall free energy change in going from the ground state, $(E \cdot S)_C + G_{2'X}$, to the chemical transition state, $(E \cdot S \cdot G_{2'X})^{\ddagger}$ (eq 3) (*4, 35, 36*). Under these conditions, $\Delta G^{(k_c/K_m)^{G(2'X)}}_{H\ removal}$ reflects both guanosine binding ($\Delta G^{binding}_{H\ removal}$) and the subsequent phosphoryl transfer reaction ($\Delta G^{chemistry}_{H\ removal}$) (eq 4).

$$\underbrace{(E \cdot S)_C + G_{2'X} \rightarrow (E \cdot S \cdot G_{2'X})_C}_{Binding} \rightarrow \underbrace{(E \cdot S \cdot G_{2'X})^{\ddagger}}_{Catalysis} \rightarrow (E \cdot P \cdot G_{2'X}A) \qquad (3)$$

$$(k_c/K_m)^{G(2'X)}$$

$$\Delta G^{(k_c/K_m)^{G(2'X)}}_{H\ removal} = \Delta G^{binding}_{H\ removal} + \Delta G^{chemistry}_{H\ removal} \qquad (4)$$

Cleavage reactions with G_{NHCH_3} were performed at concentrations (0−0.8 mM) well below the onset of the substrate inhibition (>4 mM) caused by this analogue (inset, Figure 5B). Under $(k_c/K_m)^{G(2'X)}$ conditions, G_{NHCH_3} reacts approximately 560-fold slower than G_{NH_2}. After accounting for the 10-fold effect on binding as described above ($\Delta\Delta G^{binding}_{NH_2 \rightarrow NHCH_3}$ = 1.4 kcal/mol, Figure 6B), we find that the methyl group of G_{NHCH_3} slows the reaction of the ternary complex by approximately 60-fold relative to the reaction of the G_{NH_2} ternary complex ($\Delta\Delta G^{chemistry}_{NH_2 \rightarrow NHCH_3} = 2.4$ kcal/mol). Thus, there is an additional energetic penalty from the 2′-NH_2 to 2′-$NHCH_3$ mutation in the transition state relative to the penalty associated with ground-state binding. As the $(E \cdot S \cdot G_{2'X})_C$ complex approaches the transition state, the nucleophilic oxygen atom moves within covalent bonding distance of the scissile phosphate, and the phosphorus atom presumably rehybridizes from a tetrahedral to a trigonal bipyramidal geometry. Additionally, negative charge accumulates on the phosphate oxygens in the transition state. These spatial and electronic changes alone could render the active site less able to accommodate the bulky, nonpolar methyl group in the transition state relative to the ground state. The greater energetic penalty for the methyl group also could reflect a local conformational change within the active site as the ternary complex approaches the chemical transition state.

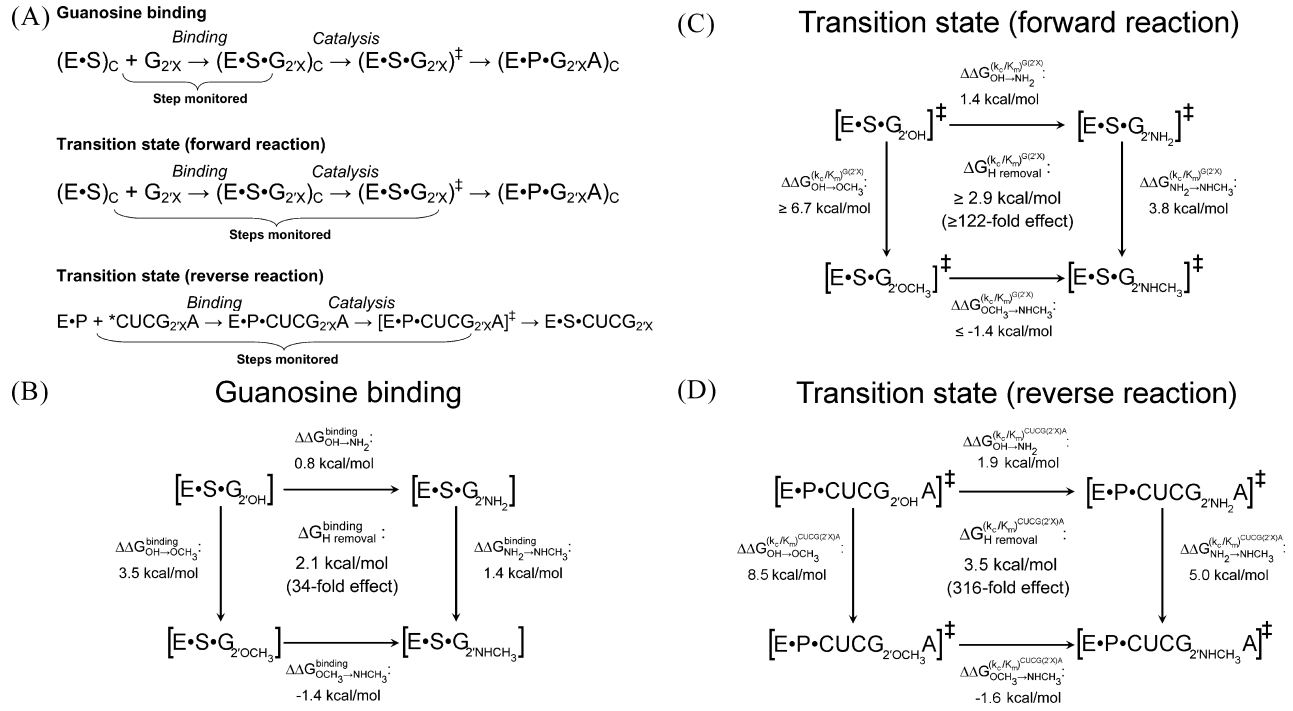

FIGURE 6: Atomic mutation cycle analysis of guanosine binding and reactivity in the forward and reverse ribozyme reactions. (A) Reaction schemes highlighting the reaction steps probed by atomic mutation cycle analysis: guanosine binding, the transition state for the forward cleavage reaction under $(k_c/K_m)^{G(2'X)}$ conditions, and the transition state for the reverse cleavage reaction under $(k_c/K_m)^{CUCG(2'X)A}$ conditions. (B) The guanosine 2′-hydroxyl donates a hydrogen bond in the ground state within the $(E\cdot S\cdot G)_C$ ternary complex. $\Delta\Delta G^{binding}_{X\rightarrow Y}$ values reflect differences in binding affinities to the $(E\cdot S)_C$ complex for $G_{2'X}$ relative to $G_{2'Y}$; $\Delta\Delta G^{binding}_{X\rightarrow Y} = RT\ln(K_d^{G(2'X)}/K_d^{G(2'Y)})$, where $K_d^{G(2'X)}$ and $K_d^{G(2'Y)}$ are the observed binding affinities for guanosine analogues with X and Y groups at the 2′-position, respectively, as reported in Table 2. All affinities were measured at 30 °C. (C) A hydrogen bond donated by the guanosine 2′-hydroxyl group contributes to transition-state stabilization. $\Delta\Delta G^{(k_c/K_m)^{G(2'X)}}_{X\rightarrow Y}$ values reflect differences in reactivity for $G_{2'X}$ relative to $G_{2'Y}$ under $(k_c/K_m)^{G(2'X)}$ conditions; $\Delta\Delta G^{(k_c/K_m)^{G(2'X)}}_{X\rightarrow Y} = RT\ln[(k_c/K_m)^{G(2'X)}/(k_c/K_m)^{G(2'Y)}]$, where $(k_c/K_m)^{G(2'X)}$ and $(k_c/K_m)^{G(2'Y)}$ are the observed reactivities for guanosine analogues with X and Y groups at the 2′-position, respectively, as reported in Table 3. All $(k_c/K_m)^{G(2'X)}$ values were measured at 30 °C. (D) A hydrogen bond donated by the guanosine 2′-hydroxyl group contributes to transition-state stabilization in the reverse reaction. $\Delta\Delta G^{(k_c/K_m)^{CUCG(2'X)A}}_{X\rightarrow Y}$ values reflect differences in reactivity for $CUCG_{2'X}A$ relative to $CUCG_{2'Y}A$ under $(k_c/K_m)^{CUCG(2'X)A}$ conditions; $\Delta\Delta G^{(k_c/K_m)^{CUCG(2'X)A}}_{X\rightarrow Y} = RT\ln[(k_c/K_m)^{CUCG(2'X)A}/(k_c/K_m)^{CUCG(2'Y)A}]$, where $(k_c/K_m)^{CUCG(2'X)A}$ and $(k_c/K_m)^{CUCG(2'Y)A}$ are the observed reactivities for substrates with guanosine analogues with X and Y groups at the 2′-position, respectively, as reported in Table 4. All $(k_c/K_m)^{CUCG(2'X)A}$ values were measured at 30 °C.

Table 3: Second Order Rate Constants $[(k_c/K_m)^{G(2'X)}]$ for the Reaction of Guanosine Analogues

analogue	$(k_c/K_m)^{G(2'X)}$ (M^{-1} min^{-1})	$(k_c/K_m)^{G(2'X)}/(k_c/K_m)^{G(2'OH)}$
G_{OH}	2700 ± 400	(1)
G_{OCH_3}	≤0.04[a]	$\leq 1.5\times10^{-5}$
G_{NH_2}	246 ± 7	9×10^{-2}
G_{NHCH_3}	0.44 ± 0.05[b]	1.6×10^{-4}

[a] $(k_c/K_m)^{G(2'X)}$ for G_{OCH_3} is an upper limit, as described in the text. [b] $(k_c/K_m)^{G(2'X)}$ for G_{NHCH_3} was measured at low concentrations of G_{NHCH_3}, below the onset of substrate inhibition at high G_{NHCH_3} concentrations.

Because we do not observe substrate cleavage by G_{OCH_3}, we may only calculate a lower limit for the effect of the 2′-OH to 2′-OCH_3 modification on the transition state ($\Delta\Delta G^{chemistry}_{OH\rightarrow OCH_3}$). Assuming that G_{OCH_3} reacts at least 10-fold slower than does G_{NHCH_3}, $(k_c/K_m)^{G(2'OCH_3)}$ must be at least 68,000-fold smaller than $(k_c/K_m)^{G(2'OH)}$ (Table 3). After accounting for the 340-fold weaker binding of G_{OCH_3} compared to that of G_{OH} ($\Delta\Delta G^{binding}_{OH\rightarrow OCH_3} = 3.5$ kcal/mol, Figure 6B), we calculate that the methoxy group imparts at least a 200-fold deleterious effect on the reaction of the $(E\cdot S\cdot G_{OCH_3})_C$ ternary complex relative to the reaction of the $(E\cdot S\cdot G_{OH})_C$ ternary complex ($\Delta\Delta G^{chemistry}_{OH\rightarrow OCH_3} \geq 3.2$ kcal/mol). From the difference in $(k_c/K_m)^{G(2'X)}$ values resulting from the 2′-OH to 2′-OCH_3 mutation ($\Delta\Delta G^{(k_c/K_m)^{G(2'X)}}_{OH\rightarrow OCH_3} \geq 6.7$ kcal/mol) and the 2′-NH_2 to 2′-$NHCH_3$ mutation ($\Delta\Delta G^{(k_c/K_m)^{G(2'X)}}_{NH_2\rightarrow NHCH_3} = 3.8$ kcal/mol), we calculate $\Delta G^{(k_c/K_m)^{G(2'X)}}_{H\ removal}$ as ≥ 2.9 kcal/mol (Figure 6C). The ≥ 0.8 kcal/mol difference between $\Delta G^{(k_c/K_m)^{G(2'X)}}_{H\ removal}$ and $\Delta G^{binding}_{H\ removal}$ (≥2.9 kcal/mol − 2.1 kcal/mol = ≥ 0.8 kcal/mol) suggests that a hydrogen bond donated by the guanosine 2′-hydroxyl group in the ground-state ternary complex may become stronger in the transition state ($\Delta G^{chemistry}_{H\ removal} \geq 0.8$ kcal/mol).

Atomic Mutation Cycle Analysis of Guanosine Reactivity in the Reverse Cleavage Reaction. To obtain a more precise estimate for the energetic contribution of the hydrogen atom upon going from the ground-state ternary complex to the chemical transition state, we employed a reaction that mimics the second step of group I intron self-splicing, wherein an oligonucleotide product analogue (P, CCCUCU) attacks a radiolabeled 3′-splice site analogue (*$CUCG_{2'X}A$) (eq. 5) (*37–42*).

$$\underbrace{E\cdot P + {}^*CUCG_{2'X}A \rightarrow E\cdot P\cdot {}^*CUCG_{2'X}A \rightarrow [E\cdot P\cdot {}^*CUCG_{2'X}A]^{\ddagger}}_{(k_c/K_m)^{CUCG(2'X)A}} \rightarrow E\cdot S\cdot {}^*CUCG_{2'X} \quad (5)$$

Radiolabeling of the substrates containing the guanosine analogues allows a more sensitive measure of their reactivity in the ribozyme reactions. To keep the chemical step rate-limiting in reactions with $CUCG_{OH}A$ and $CUCG_{NH_2}A$, we used a product analogue containing 2′-deoxythymidine at the

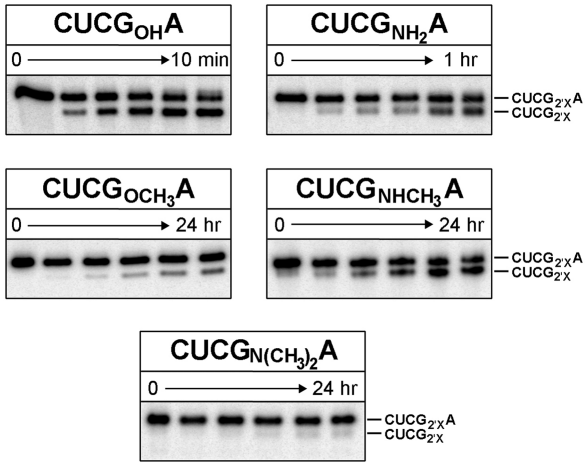

FIGURE 7: Activity of CUCG$_{2'X}$A substrates in the reverse cleavage reaction. 5′-Labeled CUCG$_{2'X}$A substrates were reacted with product oligonucleotides rP and −1d,rP (Table 1) as described in Materials and Methods. CUCGA and CUCG$_{NH_2}$A were reacted with −1d,rP, and CUCG$_{OCH_3}$A, CUCG$_{NHCH_3}$A, and CUCG$_{N(CH_3)_2}$A were reacted with rP as described in the text. All CUCG$_{2'X}$A substrates except for CUCG$_{N(CH_3)_2}$A exhibited specific cleavage downstream of the guanosine residue, with $(k_c/K_m)^{CUCG(2'X)A}$ values as reported in Table 4.

Table 4: Second Order Rate Constants $[(k_c/K_m)^{CUCG(2'X)A}]$ for the Reaction of Guanosine Analogues in the Reverse Cleavage Reaction[a]

CUCG$_{2'X}$A	$(k_c/K_m)^{CUCG(2'X)A}$ (10^2 M^{-1} min^{-1})	$(k_c/K_m)^{CUCG(2'X)A}$/ $(k_c/K_m)^{CUCG(2'OH)A}$
2′-OH	2100 ± 100	(1)
2′-OCH$_3$	1.8 ± 0.1[b]	
	0.0015 ± 0.0001[c]	*7 × 10^{-7}*
2′-NH$_2$	90 ± 10	0.04
2′-NHCH$_3$	25 ± 3[b]	
	0.021 ± 0.003[c]	*1 × 10^{-5}*

[a] $(k_c/K_m)^{CUCG(2'X)A}$ was measured in the presence of 1 μM E•P complex at pH 8, as described in Materials and Methods. [b] Measured in reaction with an all-ribose product oligonucleotide (rP, Table 1). [c] Calculated value for $(k_c/K_m)^{CUCG(2'X)A}$ in reaction with −1d,rP; previous work has shown that removal of the 2′-hydroxyl at the U$_{-1}$ position decelerates the chemical step by 1188-fold in the reverse reaction (*43*).

−1 position (−1d,rP, Table 1); this modification slows the chemical step ~1200-fold without affecting other reaction steps (*43*). In reactions with −1d,rP, both CUCG$_{OH}$A and CUCG$_{NH_2}$A exhibit log-linear pH dependencies up to pH 8, consistent with chemistry being the rate-limiting step (data not shown) (*34, 44*). However, as CUCG$_{OCH_3}$A or CUCG$_{NHCH_3}$A show no detectable cleavage in the presence of −1d,rP, we used the faster reacting all-ribose product analogue (rP, Table 1) to monitor the reactivity of these substrates. Under these conditions, both CUCG$_{NHCH_3}$A and CUCG$_{OCH_3}$A are cleaved by rP (Figure 7). The resulting $(k_c/K_m)^{CUCG(2'X)A}$ values were divided by the reported differential in reactivity between rP and −1d,rP (*43*) to allow comparison to rates measured for CUCG$_{OH}$A and CUCG$_{NH_2}$A in reactions with −1d,rP (Table 4).[6] The normalized rate constants indicate that CUCG$_{OCH_3}$A reacts approximately 1.4 × 10^6-fold more slowly than does CUCG$_{OH}$A, reflecting an energetic cost of 8.5 kcal/mol upon installation of the methyl group ($\Delta\Delta G^{(k_c/K_m)^{CUCG(2'X)A}}_{OH\rightarrow OCH_3}$, Figure 6D). In contrast, CUCG$_{NHCH_3}$A reacts only 4400-fold more slowly than CUCG$_{NH_2}$A, reflecting an energetic cost of 5.0 kcal/mol upon methyl group incorporation ($\Delta\Delta G^{(k_c/K_m)^{CUCG(2'X)A}}_{NH_2\rightarrow NHCH_3}$, Figure 6D). The difference in these energetic penalties yields a value for $\Delta G^{(k_c/K_m)^{CUCG(2'X)A}}_{H\ removal}$ of 3.5 kcal/mol under $(k_c/K_m)^{CUCG(2'X)A}$ conditions (Figure 6D), consistent with the limit set for $\Delta G^{(k_c/K_m)^{G(2'X)}}_{H\ removal}$ in the forward reaction, ≥2.9 kcal/mol, under $(k_c/K_m)^{G(2'X)}$ conditions.

As a final control, we assayed the reactivity of a 3′-splice site analogue incorporating 2′-dimethylaminoguanosine at the cleavage site (CUCG$_{N(CH_3)_2}$A, Table 1). If the greater reactivity of CUCG$_{NHCH_3}$A relative to CUCG$_{OCH_3}$A arises from an energetic contribution by the heteroatom bound hydrogen, then CUCG$_{N(CH_3)_2}$A, which lacks this hydrogen atom, should react slower than CUCG$_{NHCH_3}$A. Under reaction conditions where both CUCG$_{NHCH_3}$A and CUCG$_{OCH_3}$A react to a significant extent, CUCG$_{N(CH_3)_2}$A does not react (Figure 7). Although we cannot eliminate the possibility that the slower reactivity of CUCG$_{N(CH_3)_2}$A relative to CUCG$_{NHCH_3}$A reflects steric clash from the larger dimethylamino group, the observation is consistent with a model in which the heteroatom-bound hydrogen atom contributes to transition-state stabilization.

DISCUSSION

Both protein and RNA-based enzymes use networks of noncovalent interactions to bind substrates and catalyze chemical transformations. Dissecting the character, location, and specific role of these interactions represents a key step in developing an atomic-level understanding of biological catalysis. Toward developing this understanding for the *Tetrahymena* ribozyme, we have used an atomic mutation cycle to explore whether the 2′-hydroxyl group of the guanosine nucleophile donates a hydrogen bond. The cycle attributes the energetic differences between the 2′-OH to 2′-OCH$_3$ mutation and the 2′-NH$_2$ to 2′-NHCH$_3$ mutation to the removal of a heteroatom-bound hydrogen atom ($\Delta G_{H\ removal}$). We find that the 2′-OH to 2′-OCH$_3$ mutation weakens guanosine binding by 2.1 kcal/mol more than does the 2′-NH$_2$ to 2′-NHCH$_3$ mutation, suggesting that the guanosine 2′-hydroxyl group donates a hydrogen bond when bound to the ribozyme. This hydrogen bond remains as the ground-state (E•S•G$_{2'OH}$)$_C$ complex proceeds to the transition state and may become stronger, as suggested by $\Delta G^{(k_c/K_m)^{G(2'X)}}_{H\ removal}$ in the forward reaction and $\Delta G^{(k_c/K_m)^{CUCG(2'X)A}}_{H\ removal}$ in the reverse reaction being at least 0.8 kcal/mol greater than $\Delta G^{binding}_{H\ removal}$. These findings extend our understanding of cofactor recognition and catalysis by the group I intron and provide an additional feature by which to evaluate the relationship between crystal structures and the structure of the transition state.

While this work strongly suggests that the 2′-hydroxyl of the guanosine cofactor donates a functionally important hydrogen bond, the values of $\Delta G^{binding}_{H\ removal}$ and $\Delta G^{chemistry}_{H\ removal}$ need not reflect the true energetic contribution of this hydroxyl-mediated hydrogen bond. Our analysis assumes that the differences between the 2′-NH$_2$ to 2′-NHCH$_3$ mutation and the 2′-OH to 2′-OCH$_3$ mutation arise predominantly from changes in hydrogen-bonding ability. However, other features of these nucleotides could affect binding and catalysis and therefore contribute to the observed $\Delta G_{H\ removal}$, including differences in volume, hydrophobicity, electronegativity,

[6] As CUCG$_{OCH_3}$A and CUCG$_{NHCH_3}$A react with rP slower than CUCG$_{OH}$A reacts with −1d,rP, the chemical step likely limits the rate of rP-mediated cleavage of CUCG$_{OCH_3}$A and CUCG$_{NHCH_3}$A.

sugar pucker preference, and the ability to coordinate a catalytic metal ion (M_C, Figure 1A). Nevertheless, the cycle provides a better signature for the role of hydrogen bonding than would the simple comparison of G_{OCH_3} to G_{NHCH_3}. For example, contributions from changes in volume, hydrophobicity, electronegativity, and sugar pucker preferences predominantly offset each other across the verticals of the cycle (see Supporting Information). Regarding the ability to coordinate M_C, we have shown that the 2′-NH_2 and 2′-$NHCH_3$ groups give similar Mn^{2+} rescue profiles (Figure 4), suggesting that 2′-$NHCH_3$ group coordinates to M_C. While we have no direct test to determine whether 2′-OCH_3 coordinates M_C, the limited data available suggest that 2′-OCH_3 may act as a stronger ligand donor than the hydroxyl group (see footnote 2 and references therein).

The 2′-NH_2/2′-$NHCH_3$ comparison may overestimate the cost of methyl group installation if the presence of the methyl group deleteriously affects the ability of the 2′-$NHCH_3$ group to donate a hydrogen bond relative to the 2′-NH_2 group (due to steric constraints, conformational effects such as changes in ribose conformation, or other factors both in solution and within the ribozyme active site), resulting in an underestimation of the energetic cost of hydrogen atom removal. Alternatively, the relatively large energetic penalty induced by the methyl group may cause local changes in structure that could result in favorable non-native interactions. As a consequence, it remains formally possible that a hydrogen bond donated by the $-NHCH_3$ group contributes to binding and catalysis in the presence of the methyl group, but not in its absence.

Despite these possible limitations, several observations support the use of $\Delta G^{\text{binding}}_{\text{H removal}}$, $\Delta G^{(k_c/K_m)^{G(2'X)}}_{\text{H removal}}$, and $\Delta G^{(k_c/K_m)^{CUCG(2'X)A}}_{\text{H removal}}$ to infer that the guanosine 2′-hydroxyl group donates a hydrogen bond. First, similarly large energetic effects were observed previously for AMC modifications of the 2′-hydroxyl group at U_{-1}, and the conclusions derived from that analysis agree with those derived from independent functional studies (*20, 30, 34, 45*) and from the structure of the *Azoarcus* group I intron (*10, 12*). Second, evidence suggests that many of the previously established catalytic interactions remain important in the transition state despite the presence of the methyl group. For example, as described here, the interaction between M_C and the guanosine 2′-substituent still occurs, and the faster reaction of $CUCG_{OCH_3}A$ with rP than with −1d,rP indicates that in the transition state the 2′-hydroxyl group at the U_{-1} position maintains a catalytic contribution. Additionally, a double-modified guanosine analogue bearing a 3′-sulfur leaving group and an adjacent 2′-OCH_3 group undergoes specific metal ion rescue, suggesting that the interaction between the guanosine 3′-position and a catalytic metal ion still contributes to catalysis in the presence of a methyl group (Lea, C. R., Sengupta, R. N., and Piccirilli, J. A., unpublished experiments). These observations suggest that the transition-state structures for reaction of G_{OCH_3} and G_{NHCH_3} do not differ drastically from the transition-state structure for the native reaction.

Our findings underscore a recurring feature of the interaction network at the group I intron active site: multidentate interactions involving the oxygen atoms of the transferred phosphoryl group and the flanking 2′-hydroxyl groups (Figure 1). The U_{-1} 3′-oxygen coordinates to M_A and accepts a hydrogen bond from the adjacent 2′-hydroxyl group (*16, 19, 20*), the nonbridging *pro*-S_P phosphate oxygen coordinates to M_A and M_C (*21, 46*), the U_{-1} 2′-hydroxyl group donates a hydrogen bond to the adjacent 3′-oxygen and accepts a hydrogen bond from the 2′-hydroxyl of A207 (*20, 34, 45*), and the guanosine 2′-hydroxyl group coordinates to M_C (*18, 19, 27*) and, as suggested herein, donates a hydrogen bond. The adjacent guanosine 3′-oxygen interacts with a metal ion, but it remains unclear whether this interaction involves M_C, M_B, or both metal ions (*12, 17, 19*).

RNA-based enzymes commonly use the 2′-hydroxyl groups that flank the reaction center for catalysis. The *Tetrahymena* group I ribozyme uses hydroxyl groups from both the guanosine (*18, 22, 26, 27*) and the cleavage site uridine (*20, 30, 34, 45*). For catalysis of exon ligation, the ai5γ group II intron uses the 2′-hydroxyl group at the intron/3′-exon boundary (*47*) and to a lesser extent the 2′-hydroxyl group at the 5′-exon/intron boundary (*29, 48*). RNase P uses the cleavage site 2′-hydroxyl group for catalysis of pre-tRNA cleavage (*49–51*), and the ribosome uses the 2′-hydroxyl at the 3′-terminus of peptidyl-tRNA for catalysis of peptidyl transfer (*52, 53*). However, the molecular basis of these catalytic contributions and whether they involve multidentate interactions as in the *Tetrahymena* ribozyme awaits further mechanistic dissection.

With the guanosine 2′-hydroxyl group identified as an important hydrogen bond donor, the next steps toward understanding this functional group's role in catalysis involve identifying the corresponding hydrogen bond acceptor and addressing how the hydrogen bond interaction contributes to function. One plausible candidate for the hydrogen-bonding partner of the guanosine 2′-hydroxyl is the adjacent 3′-oxygen, which could participate in a hydrogen bond interaction analogous to the one previously identified at the cleavage site uridine (Figure 1) (*20*). To test this possibility, we synthesized $CUCG_{3'S,2'OH}A$ and $CUCG_{3'S,2'OCH_3}A$ to assess $\Delta\Delta G^{(k_c/K_m)^{CUCG(2'X)A}}_{OH\rightarrow OCH_3}$ in the context of a 3′-phosphorothiolate substrate. Compared to oxygen, sulfur is a weaker hydrogen bond acceptor. Therefore, if the 2′-hydroxyl group donates a hydrogen bond to the adjacent leaving group, we would expect the 2′-OH to 2′-OCH_3 mutation to cost less for the 3′-sulfur substrate than for the 3′-oxygen substrate (*20*). We found that the 2′-OH to 2′-OCH_3 mutation had the same effect for both the 3′-O and the 3′-S substrates, suggesting the absence of a hydrogen bond between the guanosine 2′-hydroxyl group and the adjacent 3′-oxygen atom (*54*).

The available group I intron crystal structures implicate another potential hydrogen-bonding partner, the universally conserved A261 nucleotide within the J6/7 region of the intron. In the *Tetrahymena* and Twort ribozyme crystals, the 2′-OH of A261 resides within acceptable hydrogen-bonding distance of the guanosine 2′-hydroxyl and N3 nitrogen (Table 5), possibly forming a ribose zipper interaction (Figure 8) (*11, 13*). This possibility has been noted and discussed previously by Golden et al. in the context of the *Twort* ribozyme (*13*). Interestingly, the A261 equivalent in the *Azoarcus* ribozyme (A127) lies just outside what might be considered acceptable hydrogen-bonding distance from the ωG 2′-hydroxyl group (*10, 12*). An interaction between A261 and the guanosine nucleophile could serve to constrain the loop at the top of P7, including J6/7, in a conformation necessary for catalysis. Consistent with the structural evidence for this putative ribose zipper interaction, nucleotide

Table 5: Crystallographic Distances between Proposed Hydrogen Bonding Partners in a $\omega G_{2'OH} \rightarrow A261_{2'OH}$ Ribose Zipper

ribozyme	pdb ID	resolution (Å)	distance (Å)[a]	
			$\omega G_{2'OH} \rightarrow A261_{2'OH}$	$A261_{2'OH} \rightarrow \omega G_{N3}$
Tetrahymena	1X8W(A)[b]	3.80	3.2	4.0
	1X8W(B)[b]	3.80	2.6	3.6
	1X8W(C)[b]	3.80	3.3	2.8
	1X8W(D)[b]	3.80	2.8	3.2
Azoarcus[c]	1U6B	3.10	4.1	2.8
	1ZZN	3.37	4.9	4.3
Twort[d]	1Y0Q	3.60	3.1	2.6

[a] Distances were measured between heteroatoms using Swiss PDB Viewer (*58*). [b] The suffixes (A)−(D) denote the four *Tetrahymena* ribozyme molecules in the unit cell. [c] Distances measured from *Azoarcus* equivalent nucleotide to A261 in *Tetrahymena* (A127). [d] Distances measured from the Twort equivalent nucleotide to A261 in *Tetrahymena* (A119).

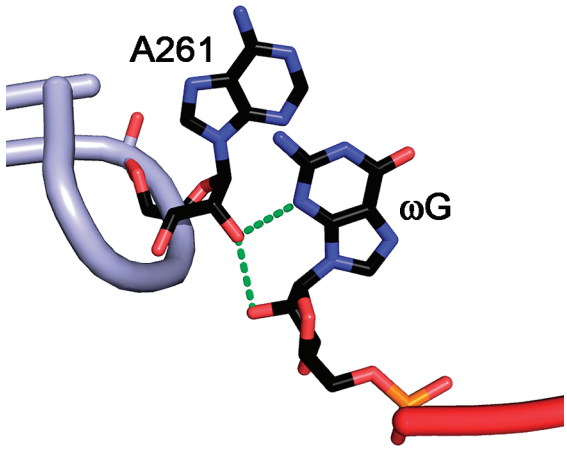

FIGURE 8: Potential ribose zipper interaction between A261 and ωG in the *Tetrahymena* ribozyme. A model of the potential ribose zipper interaction between A261 and ωG derived from molecule D, one of the four molecules reported in the asymmetric unit of the *Tetrahymena* intron crystal structure 1X8W, using Pymol (www.pymol.org). The putative hydrogen bonds between ωG (2′-hydroxyl and N3 nitrogen) and the 2′-hydroxyl of A261 are shown as dashed green lines.

analogue interference mapping of the *Tetrahymena* intron reveals that 2′-H, 2′-F, 2′-Cl, 2′-CH_3, 2′-OCH_3, and 2′-SH substituents all interfere with activity at A261 (*55, 56*), and 2′-H interference occurs at the corresponding residue A127 in the *Azoarcus* ribozyme (*57*). Residues known to form ribose zipper motifs in the independently folding P4−P6 domain exhibit identical interference profiles (*56*).

The active site of the *Tetrahymena* ribozyme mediates multiple networks of interconnected hydrogen bonds and metal ion interactions. To understand how these networks function cooperatively to impart catalysis, we must define the interactions that comprise them. Combining in-depth mechanistic analysis with a designed set of nucleotide analogues, we have explored the steric environment of the guanosine cofactor's 2′-hydroxyl group and have provided evidence that this 2′-hydroxyl group donates a functionally significant hydrogen bond. This hydrogen bond, which occurs both in the ground state and transition state, may help to align the catalytic groups at the active site. These findings advance our understanding of cofactor recognition by the group I intron.

ACKNOWLEDGMENT

We thank Dr. N.-S. Li and Dr. J. Lu for nucleotide and oligonucleotide synthesis. We thank C. Lea and J. Frederiksen for assistance with substrate preparation and kinetic measurements, and J. Olvera for assistance with ribozyme preparation and technical advice. We thank Professor D. Herschlag and members of the Piccirilli laboratory for comments and discussion.

SUPPORTING INFORMATION AVAILABLE

Characterization of the protonation state of G_{NH_2}, G_{NHCH_3}, $CUCG_{NH_2}A$, and $CUCG_{NHCH_3}A$; binding studies of $CUCG_{OH}$ and $CUCG_{OCH_3}$; Mn^{2+} stimulation of $CUCG_{OCH_3}A$ reactivity; details of Mn^{2+} rescue analysis; details of G_{NHCH_3} reactivity and inhibition analysis; and comparison of properties for AMC guanosine analogues. This material is available free of charge via the Internet at http://pubs.acs.org.

REFERENCES

1. Kappes, M. M., and Staley, R. H. (1982) Relative bond-dissociation energies for 2-ligand complexes of Ni+ with organic-molecules in the gas-phase. *J. Am. Chem. Soc. 104*, 1813–1819.
2. Hancock, R. D., and Martell, A. E. (1989) Ligand design for selective complexation of metal-ions in aqueous-solution. *Chem. Rev. 89*, 1875–1914.
3. Shan, S. O., and Herschlag, D. (2000) An unconventional origin of metal-ion rescue and inhibition in the Tetrahymena group I ribozyme reaction. *RNA 6*, 795–813.
4. Herschlag, D., and Cech, T. R. (1990) Catalysis of RNA cleavage by the *Tetrahymena thermophila* ribozyme. 1. Kinetic description of the reaction of an RNA substrate complementary to the active site. *Biochemistry 29*, 10159–10171.
5. Narlikar, G. J., Bartley, L. E., Khosla, M., and Herschlag, D. (1999) Characterization of a local folding event of the Tetrahymena group I ribozyme: effects of oligonucleotide substrate length, pH, and temperature on the two substrate binding steps. *Biochemistry 38*, 14192–14204.
6. Hougland, J. L., Piccirilli, J. A., Forconi M., Lee J., and Herschlag, D. (2006) How the Group I Intron Works: A Case Study of RNA Structure and Function, in *The RNA World* (Gesteland, R. F., Cech, T., and Atkins, J. F., Eds.) pp 133−205, Cold Spring Harbor Laboratory Press, Cold Spring Harbor, New York.
7. Herschlag, D., Eckstein, F., and Cech, T. R. (1993) Contributions of 2′-hydroxyl groups of the RNA substrate to binding and catalysis by the Tetrahymena ribozyme. An energetic picture of an active site composed of RNA. *Biochemistry 32*, 8299–8311.
8. Zaug, A. J., Been, M. D., and Cech, T. R. (1986) The Tetrahymena ribozyme acts like an RNA restriction endonuclease. *Nature 324*, 429–433.
9. Zaug, A. J., Grosshans, C. A., and Cech, T. R. (1988) Sequence-specific endoribonuclease activity of the Tetrahymena ribozyme: enhanced cleavage of certain oligonucleotide substrates that form mismatched ribozyme-substrate complexes. *Biochemistry 27*, 8924–8931.
10. Adams, P. L., Stahley, M. R., Kosek, A. B., Wang, J., and Strobel, S. A. (2004) Crystal structure of a self-splicing group I intron with both exons. *Nature 430*, 45–50.

11. Guo, F., Gooding, A. R., and Cech, T. R. (2004) Structure of the Tetrahymena ribozyme: base triple sandwich and metal ion at the active site. *Mol. Cell 16*, 351–362.
12. Stahley, M. R., and Strobel, S. A. (2005) Structural evidence for a two-metal-ion mechanism of group I intron splicing. *Science 309*, 1587–1590.
13. Golden, B. L., Kim, H., and Chase, E. (2005) Crystal structure of a phage Twort group I ribozyme-product complex. *Nat. Struct. Mol. Biol. 12*, 82–89.
14. Stahley, M. R., and Strobel, S. A. (2006) RNA splicing: group I intron crystal structures reveal the basis of splice site selection and metal ion catalysis. *Curr. Opin. Struct. Biol. 16*, 319–326.
15. Vicens, Q., and Cech, T. R. (2006) Atomic level architecture of group I introns revealed. *Trends Biochem. Sci. 31*, 41–51.
16. Piccirilli, J. A., Vyle, J. S., Caruthers, M. H., and Cech, T. R. (1993) Metal-ion catalysis in the *Tetrahymena* ribozyme reaction. *Nature 361*, 85–88.
17. Weinstein, L. B., Jones, B. C., Cosstick, R., and Cech, T. R. (1997) A second catalytic metal ion in group I ribozyme. *Nature 388*, 805–808.
18. Shan, S. O., and Herschlag, D. (1999) Probing the role of metal ions in RNA catalysis: kinetic and thermodynamic characterization of a metal ion interaction with the 2′-moiety of the guanosine nucleophile in the *Tetrahymena* group I ribozyme. *Biochemistry 38*, 10958–10975.
19. Shan, S., Yoshida, A., Sun, S., Piccirilli, J. A., and Herschlag, D. (1999) Three metal ions at the active site of the *Tetrahymena* group I ribozyme. *Proc. Natl. Acad. Sci. U.S.A. 96*, 12299–12304.
20. Yoshida, A., Shan, S., Herschlag, D., and Piccirilli, J. A. (2000) The role of the cleavage site 2′-hydroxyl in the Tetrahymena group I ribozyme reaction. *Chem. Biol. 7*, 85–96.
21. Shan, S., Kravchuk, A. V., Piccirilli, J. A., and Herschlag, D. (2001) Defining the catalytic metal ion interactions in the *Tetrahymena* ribozyme reaction. *Biochemistry 40*, 5161–5171.
22. Bass, B. L., and Cech, T. R. (1984) Specific interaction between the self-splicing RNA of Tetrahymena and its guanosine substrate: implications for biological catalysis by RNA. *Nature 308*, 820–826.
23. Michel, F., Hanna, M., Green, R., Bartel, D. P., and Szostak, J. W. (1989) The guanosine binding site of the Tetrahymena ribozyme. *Nature 342*, 391–395.
24. Karbstein, K., and Herschlag, D. (2003) Extraordinarily slow binding of guanosine to the Tetrahymena group I ribozyme: implications for RNA preorganization and function. *Proc. Natl. Acad. Sci. U.S.A. 100*, 2300–2305.
25. McConnell, T. S., Cech, T. R., and Herschlag, D. (1993) Guanosine binding to the Tetrahymena ribozyme: thermodynamic coupling with oligonucleotide binding. *Proc. Natl. Acad. Sci. U.S.A. 90*, 8362–8366.
26. Bass, B. L., and Cech, T. R. (1986) Ribozyme inhibitors: deoxyguanosine and dideoxyguanosine are competitive inhibitors of self-splicing of the Tetrahymena ribosomal ribonucleic acid precursor. *Biochemistry 25*, 4473–4477.
27. Sjogren, A. S., Pettersson, E., Sjoberg, B. M., and Stromberg, R. (1997) Metal ion interaction with cosubstrate in self-splicing of group I introns. *Nucleic Acids Res. 25*, 648–653.
28. Moran, S., Kierzek, R., and Turner, D. H. (1993) Binding of guanosine and 3′ splice site analogues to a group I ribozyme: interactions with functional groups of guanosine and with additional nucleotides. *Biochemistry 32*, 5247–5256.
29. Gordon, P. M., Fong, R., Deb, S. K., Li, N. S., Schwans, J. P., Ye, J. D., and Piccirilli, J. A. (2004) New strategies for exploring RNA's 2′-OH expose the importance of solvent during group II intron catalysis. *Chem. Biol. 11*, 237–246.
30. Hougland, J. L., Deb, S. K., Maric, D., and Piccirilli, J. A. (2004) An atomic mutation cycle for exploring RNA's 2′-hydroxyl group. *J. Am. Chem. Soc. 126*, 13578–13579.
31. Das, S. R., Fong, R., and Piccirilli, J. A. (2005) Nucleotide analogues to investigate RNA structure and function. *Curr. Opin. Chem. Biol. 9*, 585–593.
32. Dai, Q., Deb, S. K., Hougland, J. L., and Piccirilli, J. A. (2006) Improved synthesis of 2′-amino-2′-deoxyguanosine and its phosphoramidite. *Bioorg. Med. Chem. 14*, 705–713.
33. Chamberlin, S. I., and Weeks, K. M. (2000) Mapping local nucleotide flexibility by selective acylation of 2′-amine substituted RNA. *J. Am. Chem. Soc. 122*, 216–224.
34. Herschlag, D., Eckstein, F., and Cech, T. R. (1993) The importance of being ribose at the cleavage site in the Tetrahymena ribozyme reaction. *Biochemistry 32*, 8312–8321.
35. Herschlag, D., Piccirilli, J. A., and Cech, T. R. (1991) Ribozyme-catalyzed and nonenzymatic reactions of phosphate diesters: rate effects upon substitution of sulfur for a nonbridging phosphoryl oxygen atom. *Biochemistry 30*, 4844–4854.
36. Cech, T. R., Herschlag, D., Piccirilli, J. A., and Pyle, A. M. (1992) RNA catalysis by a group I ribozyme. Developing a model for transition state stabilization. *J. Biol. Chem. 267*, 17479–17482.
37. Zaug, A. J., and Cech, T. R. (1986) The intervening sequence RNA of Tetrahymena is an enzyme. *Science 231*, 470–475.
38. Woodson, S. A., and Cech, T. R. (1989) Reverse self-splicing of the Tetrahymena group I intron: implication for the directionality of splicing and for intron transposition. *Cell 57*, 335–345.
39. Bevilacqua, P. C., Johnson, K. A., and Turner, D. H. (1993) Cooperative and anticooperative binding to a ribozyme. *Proc. Natl. Acad. Sci. U.S.A. 90*, 8357–8361.
40. Mei, R., and Herschlag, D. (1996) Mechanistic investigations of a ribozyme derived from the Tetrahymena group I intron: insights into catalysis and the second step of self-splicing. *Biochemistry 35*, 5796–5809.
41. Bevilacqua, P. C., Sugimoto, N., and Turner, D. H. (1996) A mechanistic framework for the second step of splicing catalyzed by the Tetrahymena ribozyme. *Biochemistry 35*, 648–658.
42. Karbstein, K., Carroll, K. S., and Herschlag, D. (2002) Probing the Tetrahymena group I ribozyme reaction in both directions. *Biochemistry 41*, 11171–11183.
43. McConnell, T. S. (1995) Doctoral thesis, University of Colorado.
44. Herschlag, D., and Khosla, M. (1994) Comparison of pH dependencies of the Tetrahymena ribozyme reactions with RNA 2′-substituted and phosphorothioate substrates reveals a rate-limiting conformational step. *Biochemistry 33*, 5291–5297.
45. Strobel, S. A., and Ortoleva-Donnelly, L. (1999) A hydrogen-bonding triad stabilizes the chemical transition state of a group I ribozyme. *Chem. Biol. 6*, 153–165.
46. Yoshida, A., Sun, S., and Piccirilli, J. A. (1999) A new metal ion interaction in the *Tetrahymena* ribozyme reaction revealed by double sulfur substitution. *Nat. Struct. Biol. 6*, 318–321.
47. Gordon, P. M., Sontheimer, E. J., and Picirilli, J. A. (2000) Kinetic characterization of the second step of group II intron splicing: role of metal ions and the cleavage site 2′-OH in catalysis. *Biochemistry 39*, 12939–12952.
48. Griffin, E. A., Qin, P. Z., Michels, W. J., and Pyle, A. M. (1995) Group II intron ribozymes that cleave DNA and RNA linkages with similar efficiency. *Chem. Biol. 11*, 761–770.
49. Persson, T., Cuzic, S., and Hartmann, R. K. (2003) Catalysis by RNase P RNA: unique features and unprecedented active site plasticity. *J. Biol. Chem. 278*, 43394–43401.
50. Zahler, N. H., Sun, L., Christian, E. L., and Harris, M. E. (2005) The pre-tRNA nucleotide base and 2′-hydroxyl at N(−1) contribute to fidelity in tRNA processing by RNase P. *J. Mol. Biol. 345*, 969–985.
51. Kleineidam, R. G., Pitulle, C., Sproat, B., and Krupp, G. (1993) Efficient cleavage of pre-tRNAs by E. coli RNAse P RNA requires the 2′-hydroxyl of the ribose at the cleavage site. *Nucleic Acids Res. 21*, 1097–1101.
52. Weinger, J., Parnell, K., Dorner, S., Green, R., and Strobel, S. (2004) Substrate-assisted catalysis of peptide bond formation by the ribosome. *Nat. Struct. Mol. Biol. 11*, 1101–1106.
53. Schmeing, T., Huang, K., Kitchen, D., Strobel, S., and Steitz, T. (2005) Structural insights into the roles of water and the 2′ hydroxyl of the P site tRNA in the peptidyl transferase reaction. *Mol. Cell 20*, 437–448.
54. Lu, J., Li, N.-S., Sengupta, R. N., and Picirilli, J. A. (2008) Synthesis and biochemical application of 2′-O-methyl-3′-thioguanosine as a probe to explore group I intron catalysis. *Bioorg. Med. Chem.*, in press.
55. Ortoleva-Donnelly, L., Szewczak, A. A., Gutell, R. R., and Strobel, S. A. (1998) The chemical basis of adenosine conservation throughout the Tetrahymena ribozyme. *RNA 4*, 498–519.
56. Schwans, J. P. (2003) Doctoral thesis, The University of Chicago.
57. Strauss-Soukup, J. K., and Strobel, S. A. (2000) A chemical phylogeny of group I introns based upon interference mapping of a bacterial ribozyme. *J. Mol. Biol. 302*, 339–358.
58. Guex, N., and Peitsch, M. C. (1997) SWISS-MODEL and the Swiss-PdbViewer: An environment for comparative protein modeling. *Electrophoresis 18*, 2714–2723.

BI8000648